Available online at www.sciencedirect.com
ScienceDirect
Journal of Solid State Chemistry 180 (2007) 191–197
JOURNAL OF SOLID STATE CHEMISTRY
www.elsevier.com/locate/jssc

The metal-rich palladium chalcogenides Pd_2MCh_2 (M = Fe, Co, Ni; Ch = Se, Te): Crystal structure and topology of the electron density

Regina Pocha[a,b], Catrin Löhnert[a], Dirk Johrendt[a,*]

[a]*Department Chemie und Biochemie der Ludwig-Maximilians-Universität München, Butenandtstr. 5-13 (Haus D), D-81377 München, Germany*
[b]*Department of Chemistry, Michigan State University, East Lansing, MI 48824, USA*

Received 26 July 2006; received in revised form 26 September 2006; accepted 29 September 2006
Available online 4 October 2006

Abstract

Crystals of Pd_2MCh_2 (M = Fe, Co, Ni; Ch = Se, Te) were synthesized by heating the elements at 823–1323 K in silica ampoules under argon atmosphere. Their structures were determined by single-crystal X-ray diffraction at room temperature. The metallic compounds crystallize in a variant of the K_2ZnO_2 type (*Ibam*, $Z = 4$, Pd_2CoSe_2: $a = 5.993(1)$, $b = 10.493(2)$, $c = 5.003(1)$ Å; Pd_2FeSe_2: $a = 5.960(1)$, $b = 10.576(2)$, $c = 5.078(1)$ Å; Pd_2CoTe_2: $a = 6.305(1)$, $b = 11.100(2)$, $c = 5.234(1)$ Å; Pd_2NiTe_2: $a = 6.286(1)$, $b = 11.194(2)$, $c = 5.157(1)$ Å). One-dimensional $^1_\infty[MCh_{4/2}]$ tetrahedra chains with remarkably short M—M bonds run along [001], separated by [Pd_2] dumbbells with palladium in fivefold coordination of selenium or tellurium atoms. The structure may also be described as a filled variant of the SiS_2 type. M atoms occupy $\frac{1}{4}$ of the tetrahedral voids and the Pd atoms fill all octahedral voids in a distorted *ccp* motif of chalcogen atoms. Even though the Pd_2MCh_2 compounds are isotypic to K_2ZnO_2 from the crystallographic viewpoint, we find a different bonding situation with additional homo- and heteronuclear metal–metal bonds between the Pd and Co atoms. The electronic structures and topologies of the electron densities of Pd_2CoSe_2 and isotypic Na_2CoSe_2 are analyzed and compared by using Bader's AIM theory. Different values of topological charge transfer and electron density flatness indices uncover striking quantitative differences in the nature of chemical bonding between the metallic compound Pd_2CoSe_2 and nonmetallic Na_2CoSe_2.

Keywords: Chalcogenides; Palladium; Iron group metals; Crystal structure; Bader analysis

1. Introduction

Metal-rich chalcogenides have been a focus of interest in solid state chemistry over the past decades and numerous reviews have summarized an impressive variety of crystal structures and physical properties possible in this class of compounds [1–7]. One particular feature is the presence of so-called metal centered electrons. These electrons are not incorporated in metal–chalcogen bonding, but rather playing a fundamental role in the compounds structures and physical properties. Apart from the formation of metal–metal bonds or special phenomena like charge-density waves [8–10], it is accepted that localized or partially localized metal centered electrons are responsible for outstanding properties based on electronic correlation such as magnetism, metal–insulator transitions [11], superconductivity [12] or colossal magnetoresistance [13,14].

Up to now, metal-rich chalcogenides of the early transition elements have been investigated predominantly, leaving the crystal chemistry of such compounds of the late transition elements far less developed. This is surprising due to the fact that the metals at the end of the transition rows (groups 8–10) form numerous metal-rich binary chalcogenides. For instance, at least 15 binary nickel [15,16] or palladium [17–19] selenides and tellurides [20], among them several superconductors [21,22], are listed in the literature. In contrast to this, still no ternary nickel-palladium chalcogenide is known, and the same holds true for palladium chalcogenides with different iron group metals. In order to close this gap in crystal chemistry, we have started a systematic investigation in these systems and discovered the first metal-rich palladium selenides and tellurides with 3*d* transition metals. In this paper, we report

*Corresponding author. Fax: +49 89 2180 77431.
E-mail address: johrendt@lmu.de (D. Johrendt).

0022-4596/$ - see front matter © 2006 Elsevier Inc. All rights reserved.
doi:10.1016/j.jssc.2006.09.028

the synthesis and crystal structure of the series Pd_2MCh_2 with M = Fe, Co, Ni and Ch = Se or Te, along with a topological analysis of the calculated charge density distribution of Pd_2CoSe_2 to understand the nature of chemical bonding in these electron-rich intermetallic compounds.

2. Experimental

2.1. Synthesis

Pd_2MCh_2 samples were prepared by reacting stochiometric amounts of Pd filings (99.95%, Allgemeine Gold- und Silberscheideanstalt, Pforzheim), with Fe- (99.9%, Chempur), Co- (99.9%, Sigma-Aldrich) or Ni-Powder (99.99%, Chempur) and crushed Se- (99.999%, Chempur) or Te-pieces (99,997%, Alfa-Aesar) in silica tubes under a purified argon atmosphere. The selenides were heated for 40 h to 1223–1323 K, tellurides to 823–1023 K. After cooling to room temperature, the samples were homogenized with an agate mortar in a glove box and annealed at 1173 K (selenides) or 873 K (tellurides) for 24–120 h. The resulting dark gray powders were not sensitive to air or moisture. Single crystals with metallic luster, suitable for structure determination were selected directly from the powder samples. Semi-quantitative EDX measurements (Jeol JSM-6500F SEM with Oxford Instruments 7418 EDX- detector) confirmed the 2:1:2 composition of the crystals, and the presence of other elements was excluded as well.

2.2. Crystal structure determinations

X-ray powder patterns (STOE Stadi-P, Mo$K\alpha$-radiation, graphite-monochromator, 7°-PSD-detector, Si as external standard) were indexed using the crystallographic data from the single crystal experiments. However, unknown impurity phases were detected, especially in the case of Pd_2FeSe_2 and to smaller extent also in the other samples. Single crystal data sets were collected in the ϕ-scan mode using a STOE IPDS-1 imaging plate detector (Mo$K\alpha$-radiation, graphite monochromator) at room temperature. Numerical absorption corrections were performed with optimized crystal shapes using the X-SHAPE and X-RED programs [23,24]. The structures were solved with the direct methods program SHELXS [25] and refined with full-matrix least squares using SHELXL [26]. All final cycles included anisotropic displacement parameters.

Crystallographic data and experimental details of the data collections are listed in Table 1 and final atomic positions with equivalent displacement parameters in Table 2. Selected bond lengths are given in Table 3. Further details of the structure determinations may be obtained from: Fachinformationszentrum Karlsruhe, D-76344 Eggenstein-Leopoldshafen (Germany) by quoting the Registry No's. CSD-416512 (Pd_2NiTe_2), CSD-416513 (Pd_2CoSe_2), CSD-416514 (Pd_2CoTe_2) and CSD-416515 (Pd_2FeSe_2).

2.3. Quantum chemical calculations

Full potential DFT band structure calculations were performed for Pd_2CoSe_2 and Na_2CoSe_2 with the WIEN2k program package [27] using the FPLAPW method with a GGA exchange-correlation functional [28]. The basis sets consisted of 1273 or 2026 plane waves up to a cutoff $R_{mt}K_{max} = 8$ and 132 or 60 local orbitals for Pd_2CoSe_2 and Na_2CoSe_2, respectively. The atomic sphere radii R_{mt} were 2.0 au for Pd, Co, Se and 2.5 au for Na. Reciprocal space integrations were performed by the tetrahedron method using 45 k-points out of a $6 \times 6 \times 6$ mesh in the irreducible wedges of the Brillouin zones. All SCF-cycles converged to energy changes smaller than 10^{-4} Ryd and charge differences below 5×10^{-4}. In order to get smooth charge densities for the topological analysis, the lattice harmonics expansion for ρ for all atoms were increased up to $l = 10$ [29]. Atomic charges were assigned by integrations of the charge density within the atomic basins Ω and subtracting the nuclear charge Z of the corresponding atom.

3. Results and discussion

3.1. Crystal structures

Experimental parameters and results of the single crystal structure refinements are summarized in Tables 1 and 2, while selected interatomic distances are compiled in Table 3. The crystal structures of the Pd_2MCh_2 compounds are isotypic to K_2ZnO_2 [30]. The related compounds A_2CoSe_2 (A = Na–Cs) [31] also crystallize in this structure type. Fig. 1 shows the unit cell of Pd_2CoSe_2. Parallel chains of edge-sharing $CoSe_{4/2}$ tetrahedra run along [0,0,1] and $[\frac{1}{2},\frac{1}{2},1]$. The Co–Se bond length is 2.348(1) Å, only slightly longer than the sum of Pauling's covalent radii of 2.33 Å [32]. The Se–Co–Se angles within the tetrahedra are 115.6°, 113.4° and 99.8°, tantamount with a significant compression along the chain direction. This leads to short Co–Co distances of only 2.501(1) Å. Remarkable, these distances are even shorter than in *fcc* cobalt metal (2.503 Å). This indicates strong one-dimensional Co–Co bonding within the $^1_\infty[CoSe_{4/2}]$ chains. Palladium atoms separate the chains with only five selenium neighbors in a distorted quadratic–prismatic arrangement. Pd–Se bond lengths range from 2.475 to 2.852 Å. The shortest bonds are approximately the sum of the covalent radii (2.41 Å), whereas the longer Pd–Se distance of 2.852 Å indicates a rather weak interaction. In addition, we find one short Pd–Pd distance of 2.777(1) Å. This bond length is only 0.02 Å longer than in *fcc* palladium metal (2.75 Å) and again indicating homonuclear metal–metal bonds which lead to Pd_2 dumbbells in the structure. Finally, the coordination of the Co and Pd atoms is completed by four Co–Pd (or two Pd—Co) contacts of 2.829 Å. This interpretation of the

Table 1
Crystallographic data and structure refinements of Pd_2MCh_2

	Pd_2CoSe_2	Pd_2FeSe_2	Pd_2CoTe_2	Pd_2NiTe_2
M_r	429.65	426.57	526.93	526.71
Cell setting, space group	Orthorhombic, *Ibam* (No. 72)	Orthorhombic, *Ibam* (No. 72)	Orthorhombic, *Ibam* (No. 72)	Orthorhombic, *Ibam* (No. 72)
a (Å)	5.993(1)	5.960(1)	6.305(1)	6.286(1)
b (Å)	10.493(2)	10.576(2)	11.100(2)	11.194(2)
c (Å)	5.003(1)	5.078(1)	5.234(1)	5.157(1)
V (Å^3)	314.6(1)	320.1(1)	366.3(1)	362.9(1)
Z	4	4	4	4
D_x (g cm^{-3})	9.072	8.853	9.555	9.641
Radiation type	Mo $K\alpha_1$	Mo $K\alpha_1$	Mo $K\alpha_1$	Mo $K\alpha_1$
θ range (°)	3.9–32.9	3.3–32.8	3.7–32.9	3.7–32.8
μ mm^{-1}	39.35	38.03	29.54	30.43
Temperature (K)	295	295	295	295
Crystal form, colour	Irregular, black	Irregular, black	Irregular, black	Irregular, black
Crystal size (mm)	0.08 × 0.05 × 0.05	0.05 × 0.05 × 0.04	0.05 × 0.05 × 0.03	0.05 × 0.05 × 0.04
Diffractometer	STOE IPDS	STOE IPDS	STOE IPDS	STOE IPDS
Absorption correction	Numerical	Numerical	Numerical	Numerical
T_{min}	0.053	0.073	0.211	0.231
T_{max}	0.183	0.134	0.399	0.328
No. of measured, independent and observed reflections	2591, 297, 286	1888, 325, 281	2498, 378, 310	2198, 373, 306
Criterion for observed reflections	$I>2\sigma(I)$	$I>2\sigma\ (I)$	$I>2\sigma\ (I)$	$I>2\sigma\ (I)$
R_{int}	0.043	0.068	0.066	0.051
Range of h, k, l	$-8\leqslant h\leqslant 8$ $-15\leqslant k\leqslant 15$ $-7\leqslant l\leqslant 7$	$-9\leqslant h\leqslant 8$ $-16\leqslant k\leqslant 16$ $-7\leqslant l\leqslant 7$	$-9\leqslant h\leqslant 8$ $-16\leqslant k\leqslant 16$ $-7\leqslant l\leqslant 7$	$-9\leqslant h\leqslant 8$ $-16\leqslant k\leqslant 16$ $-7\leqslant l\leqslant 6$
Refinement on	F^2	F^2	F^2	F^2
$R[F^2>2\sigma\ (F^2)]$, $wR(F^2)$, S	0.021, 0.060, 1.30	0.026, 0.062, 1.15	0.027, 0.056, 1.02	0.027, 0.061, 1.06
No. of reflections	297	325	378	373
No. of parameters	17	17	17	17
$\Delta\rho_{max}$, $\Delta\rho_{min}$ (e Å^{-3})	1.38, −1.28	1.97, −1.67	1.99, −1.88	2.23, −1.74
Extinction coefficient	0.0044(6)	0.0013(3)	0.0013(2)	0.0010(3)

Table 2
Atom positions and equivalent displacement parameters (Å^2) of Pd_2MCh_2

		Wyck.	x	y	z	U_{eq}
Pd_2CoSe_2	Pd	8*j*	0.1243(1)	0.3883(1)	0	0.0090(2)
	Co	4*a*	0	0	$\frac{1}{4}$	0.0056(3)
	Se	8*j*	0.2152(1)	0.1441(1)	0	0.0072(2)
Pd_2FeSe_2	Pd	8*j*	0.1212(1)	0.3898(1)	0	0.0140(2)
	Fe	4*a*	0	0	$\frac{1}{4}$	0.0116(3)
	Se	8*j*	0.2093(1)	0.1463(1)	0	0.0123(2)
Pd_2CoTe_2	Pd	8*j*	0.1340(1)	0.3953(1)	0	0.0131(2)
	Co	4*a*	0	0	$\frac{1}{4}$	0.0055/3)
	Te	8*j*	0.2222(1)	0.1466(1)	0	0.0112(2)
Pd_2NiTe_2	Pd	8*j*	0.1366(1)	0.3966(1)	0	0.0156(2)
	Ni	4*a*	0	0	$\frac{1}{4}$	0.0110(2)
	Te	8*j*	0.2250(1)	0.1473(1)	0	0.0119(2)

Table 3
Selected interatomic distances (Å) in Pd_2MCh_2

	Pd_2CoSe_2	Pd_2FeSe_2	Pd_2CoTe_2	Pd_2NiTe_2
M–*Ch* (4 ×)	2.348(1)	2.358(1)	2.515(1)	2.526(1)
M–*M* (2 ×)	2.501(1)	2.539(1)	2.617(1)	2.579(1)
M–Pd (4 ×)	2.829(1)	2.840(1)	2.896(1)	2.867(1)
Pd–*Ch*	2.475(1)	2.484(1)	2.638(1)	2.634(1)
Pd–*Ch*	2.620(1)	2.629(1)	2.808(1)	2.845(1)
Pd–*Ch*(2 ×)	2.702(1)	2.759(1)	2.815(1)	2.765(1)
Pd–*Ch*	2.851(1)	2.840(1)	2.934(1)	2.938(1)
Pd–Pd	2.777(1)	2.742(1)	2.874(1)	2.884(1)

Pd_2CoSe_2 structure from the viewpoint of the shortest interatomic distances is emphasized in Fig. 2. The $^1_\infty[CoSe_{4/2}]$ chains with short Co–Co distances are linked by Pd_2 dumbbells via Pd–Se (not shown) and Pd–Co bonds.

The structures of the Pd_2MCh_2 compounds may also be described as filled variants of the SiS_2-type [33]. The iron group atoms replace the silicon atoms in $\frac{1}{4}$ of the tetrahedral holes in a distorted *ccp* motif of chalcogen atoms and the palladium atoms fill the octahedral holes

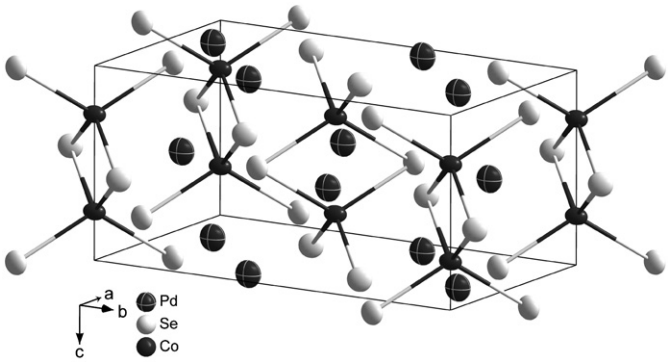

Fig. 1. Crystal structure of Pd_2CoSe_2. The one-dimensional $^1_\infty[CoSe_{4/2}]$ chains along [0,0,1] and $[\frac{1}{2},\frac{1}{2},1]$ are emphasized.

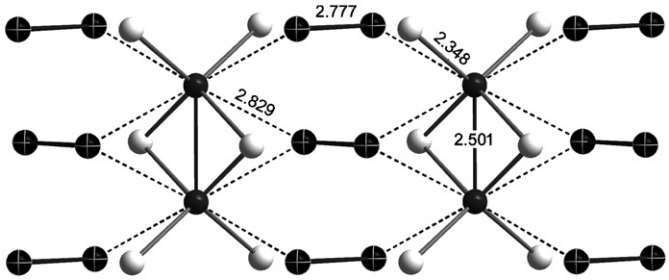

Fig. 2. Metal–metal bonding network in Pd_2CoSe_2. Connection between $^1_\infty[CoSe_{4/2}]$ tetrahedra chains via Co–Pd contacts (dotted lines) and Pd_2 dumbbells. Bond lengths are in Å.

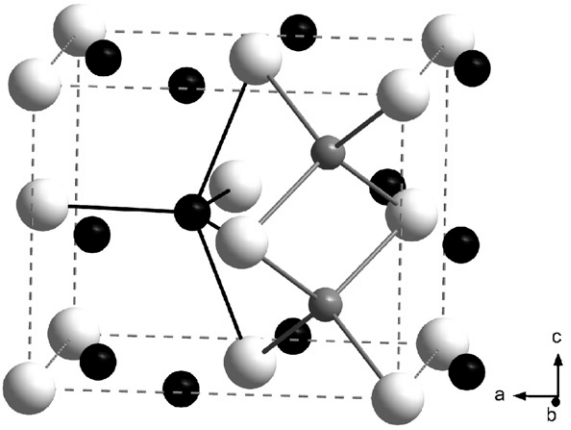

Fig. 3. Section of the crystal structure of Pd_2CoSe_2 emphasizing the distorted motif of cubic close packed Se atoms with Co in $\frac{1}{4}$ of the tetrahedral and Pd in all octahedral holes. The dotted line is a guide for the eyes and does not correspond to the unit cell.

completely. A representative section of the crystal structure is depicted in Fig. 3.

Even though Pd_2CoSe_2 and the other Pd_2MCh_2 compounds presented here are isotypic to K_2ZnO_2 from the crystallographic view, fundamental differences regarding chemical bonding and the physical properties must be recognized. The selenide Na_2CoSe_2 [31] is compositionally similar to Pd_2CoSe_2, where at first sight only the Pd atoms are substituted by Na atoms. However, the sodium atoms have a much larger radius than palladium and contribute each only one electron to the total count. Furthermore, palladium is much more electronegative ($\chi_{Pauling} = 2.2$) than sodium ($\chi_{Pauling} = 0.9$). Thus, it is straightforward to write $(Na^+)_2[(CoSe_2)^{2-}]$ emphasizing the ionic character of the compound where $(CoSe_2)^{2-}$ chains are separated by Na^+ ions. The Co–Co distance within the chains in Na_2CoSe_2 is 3.026 Å, and the shortest distance between the Na atoms is 3.808 Å. Both the Co–Co and Na–Na distances are much too long to indicate considerable bonding interaction. These bond lengths are very different compared to Pd_2CoSe_2 which exhibit a very short Co–Co bond length of 2.501 Å and a Pd–Pd bond length of 2.777 Å. This is not simply a consequence of the much smaller radius of Pd compared with Na, which shrinks the unit cell in such a way that the distances between the metal atoms become inevitably closer. The higher electron count has important consequences as well, because the metal atoms in Pd_2CoSe_2 are in a reduced oxidation state lower than 2+. These additional 'metal centered' electrons are now available for metal–metal bonding and play an important role in the stability of the structure as well as the physical properties. Na_2CoSe_2 is a typical magnetic semiconductor, however Pd_2CoSe_2 appears to be a non-magnetic metal with itinerant electrons. This was confirmed by preliminary measurements of the magnetic susceptibility and electrical conductivity. Unfortunately, the presence of impurity phases prevented a quantitative utilization of the data.

3.2. Electronic properties and chemical bonding

In order to better understand the nature of chemical bonding and the physical properties of the new Pd_2MCh_2 compounds, DFT band structure calculations of Pd_2CoSe_2 and Na_2CoSe_2 were performed for comparison. We choose the sodium compound [34] because of the smallest cell volume in the A_2CoSe_2 (A = Na–Cs) [31] series in order to minimize the atomic size effect and focus only on the differences coming from the electron count.

The total density-of-states (DOS) and the partial contributions of the atoms (PDOS) to the DOS of Pd_2CoSe_2 and Na_2CoSe_2 are depicted in Fig. 4. Initially, the DOS diagrams appear so different that one might not think these compounds are isotypic. Pd_2CoSe_2 is a metal with a relatively high DOS(ε_F) of 5 states/eV cell, which is composed by ~30% Pd-, ~40% Co- and ~13% Se- states. Nevertheless, spin polarized calculations produced non-magnetic ground-states. The reason is, that even though the DOS(ε_F) is dominated by Co states (40%) giving a Co-PDOS(ε_F) of ~1.0 states/eV · Co, this value is still only one half of Co metal and too low to fulfill the Stoner criterion [35,36] for ferromagnetic ordering ($I_S \cdot DOS(\varepsilon_F) > 1$ assuming $I_S \approx 0.5$ eV) [37]. In contrast to this, the Co-PDOS(ε_F) of a hypothetical nonmagnetic Na_2CoSe_2 (not shown in Fig. 4) is calculated to 2.3 states/eV Co and thus magnetic

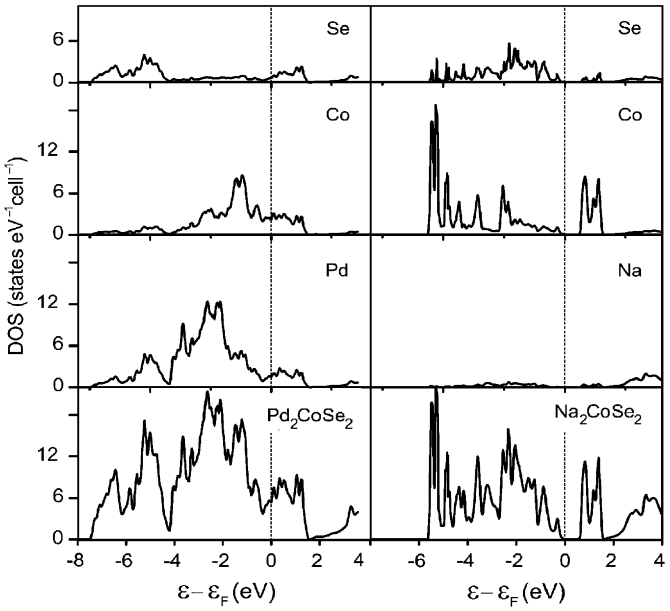

Fig. 4. Total density-of-states (DOS) curves and contributions of each atom type for Pd_2CoSe_2 (left) and Na_2CoSe_2 (right). The energy zeros are taken at the Fermi level.

ordering is expected theoretically. Indeed, experimental evidence of magnetic ordering is reported for K_2CoS_2 [31]. Subsequent spin polarized calculations of Na_2CoSe_2 converged to a magnetic moment of three unpaired spins per Co in agreement with Co^{2+}. The corresponding total DOS is shown on the right side of Fig. 4. An energy gap of ~0.5 eV is observed at the Fermi level, which emphasizes the differences in the electronic structures of Pd_2CoSe_2 and Na_2CoSe_2. The Na-PDOS curves show that sodium in Na_2CoSe_2 is almost completely ionized to Na^+, whereas the palladium orbitals are about 90% filled. Thus Pd carries, if at all, only small positive charge. Also the Co-PDOS of both compounds look quite different because the 3*d*-orbitals are strongly broadened in Pd_2CoSe_2 by the Co-$3dz^2$ overlap (Co–Co bonds), whereas magnetic splitting takes place in Na_2CoSe_2. Finally, the Se-PDOS are also very different and support the stronger ionicity of the sodium compound. Almost all Se-orbitals are filled (Se^{2-} in Na_2CoSe_2, however this is not observed in Pd_2CoSe_2. To summarize, the DOS analysis indicates fundamental differences of the electronic structures of the crystallographically isotypic compounds Pd_2CoSe_2 and Na_2CoSe_2. The latter is a normal valence compound with magnetic insulating properties, whereas Pd_2CoSe_2 appears as a *metal-rich* compound with metal-centered electrons causing strong metal–metal bonding and nonmagnetic metallic properties.

To characterize the unusual bonding situation in Pd_2CoSe_2 and compare it to Na_2CoSe_2 in more detail, topological analyses of the electron densities $\rho(r)$ following Bader's atoms-in-molecules (AIM) theory [38] were carried out. This method gives a partitioning of the crystal space into atomic basins and atomic (AIM-) charges by integration. Bonds can be characterized by a well-defined set of so called critical points (CP). A CP is a point in space where the gradient of the charge density $\vec{\nabla}\rho(r)$ vanishes. By calculating the Hessian matrix of the density at this point, one can characterize the CP by the principal curvatures (h_1, h_2, h_3) of $\rho(r)$, where $h_{1,2}$ are the curvatures perpendicular and h_3 along the bond. A CP where all curvatures are negative is a local maximum referred to as (3,3). A so-called (3,1) bond critical point (BCP) has one positive eigenvalue (h_3) at the bond path corresponding to a saddle point in $\rho(r)$. The Laplacian $L_{BCP} = \nabla^2\rho(r) = (h_1 + h_2 + h_3)$ and the density value $\rho(r)$ at the BCP provide information to classify chemical bonding. L_{BCP} is positive and large for closed shell or ionic bonding (local depletion of charge between the atoms), but negative for shared covalent interaction (local accumulation of charge between atoms). Small positive Laplacians with rather high densities are classified as intermediate interactions within AIM theory.

The results of the topological analyses of Pd_2CoSe_2 and Na_2CoSe_3 are compiled in Table 4. We detected (3,1) critical points for all bonds of Pd_2CoSe_2 listed in Table 3. In the case of Na_2CoSe_2, we find critical points only for Co–Se and the shorter Na–Se bonds < 3.2 Å. No BCP's appear between the metal atoms in Na_2CoSe_2. Even the Co–Se bonds change significantly, as seen from the smaller Laplacian in Pd_2CoSe_2 (1.28 Å^{-5}) compared with Na_2CoSe_2 (2.23 Å^5). Both values indicate closed-shell interactions, but the ionic character of the Co–Se bonds is stronger in Na_2CoSe_2. The Laplacians and densities at the BCP's of the Co–Co ($\nabla^2\rho = 1.8, \rho = 0.34$) and Pd–Pd bonds ($\nabla^2\rho = 2.2, \rho = 0.28$) in Pd_2CoSe_2 are close to those calculated for *fcc* cobalt ($\nabla^2\rho = 1.54, \rho = 0.32$) and palladium ($\nabla^2\rho = 2.6, \rho = 0.29$) metal, respectively [39]. Both results confirm the strong metal–metal bonding in Pd_2CoSe_2 from the topological viewpoint. Beyond the metal–metal bonds in Pd_2CoSe_2, the topological analysis uncovers also striking differences between the Pd–Se and Na–Se bonds. The Laplacians along the Pd–Se bond paths are larger than along Na–Se. However, higher ionicity of the Pd–Se bond cannot be inferred because the density values here are about five times larger than for Na–Se (see Table 4). Thus, in Na_2CoSe_2 typical ionic closed shell interactions between sodium and selenium were detected, but the bonds between palladium and selenium in Pd_2CoSe_2 have to be classified as intermediate from the topological view.

Atomic basins Ω are defined as regions in space traversed by trajectories of the density gradient $\vec{\nabla}\rho$ terminating at a nucleus (attractor) and enclosed inside a zero charge-density flux surface ($\vec{\nabla}\rho \cdot \vec{n} = 0$, $\vec{n}$ = face normal vector). Topological atom charges are the integrated densities inside the basins. The topology of the density together with the charges allows a classification of solids using two indices defined by Mori-Sánchez et al. [40]: (i) The global charge transfer index $c = \langle Q_\Omega / OS_\Omega \rangle$is the ratio between the actual topological charge and the expected oxidation state

Table 4
Position, curvatures, Laplacian and charge density at the (3,1) bond critical points (BCP) in Pd_2CoSe_2 and Na_2CoSe_2 (every second line) from FLAPW calculations

Bond path	d (Å)	x_{BCP}	y_{BCP}	z_{BCP}	h_1 (Å^{-5})	h_2 (Å^{-5})	h_3 (Å^{-5})	$\nabla^2\rho$ (Å^{-5})	ρ (Å^{-3})
Co–Se	2.348	0.9035	0.0658	0.3639	−1.64	−1.49	4.41	1.28	0.53
Co–Se	2.470	0.9059	0.0503	0.3604	−1.13	−1.00	4.37	2.23	0.41
Co–Co	2.501	0	0	$\frac{1}{2}$	−0.81	−0.33	2.94	1.80	0.34
Co–Co	3.252	—	—	—	—	—	—	—	—
Co–Pd	2.829	0.8180	0.9468	0.3674	−0.42	−0.11	1.89	1.36	0.23
Co–Na	3.294	—	—	—	—	—	—	—	—
Pd–Se	2.475	0.4191	0.1281	0	−1.65	−1.58	5.71	2.49	0.52
Na–Se	2.924	0.3293	0.2428	0	−0.23	−0.21	1.57	1.13	0.09
Pd–Se	2.620	0.1674	0.2679	0	−1.20	−1.20	4.88	2.48	0.40
Na–Se	2.975	0.0267	0.3705	0	−0.20	−0.19	1.41	1.03	0.08
Pd–Se	2.702	0.2940	0.1261	0.7479	−0.93	−0.71	3.95	2.31	0.33
Na–Se	3.417	—	—	—	—	—	—	—	—
Pd–Se	2.851	0.7912	0.5141	0	−0.52	−0.28	2.84	2.03	0.26
Na–Se	3.154	0.2800	0.0490	0	−0.11	−0.10	0.95	0.74	0.06
Pd–Pd	2.777	0	$\frac{1}{2}$	0	−0.73	−0.54	3.46	2.20	0.28
Na–Na	3.808	—	—	—	—	—	—	—	—

Table 5
Topological properties of the electron densities of Pd_2CoSe_2 and Na_2CoSe_2

	$Q_{Pd,\ Na}$	$V_{Pd,Na}$	$r_{Pd,Na}$	Q_{Co}	V_{Co}	r_{Co}	Q_{Se}	V_{Se}	r_{Se}	c	f
Pd_2CoSe_2	+0.06	16.03	1.37	+0.25	10.79	1.07	−0.18	17.89	1.33	0.10	0.10
Na_2CoSe_2	+0.84	11.42	1.39	+0.53	15.93	1.13	−1.10	43.79	1.70	0.61	0.03

Q, topological charge; V_Ω, volume of the atomic basin Ω (Å^3); r_Ω, topological radius (Å); c, global charge-transfer index; f, electron density flatness.

OS. (ii) The electronic flatness index f is defined as the ratio between the absolute minimum in $\rho(r)$ and the highest density at a bond critical point BCP. Elements have $c = 0$, strong ionic crystals show $c \approx 0.9$ and typical polar compounds range around 0.3–0.6. Alkaline metals show the highest flatness indices $f \approx 0.9$ and the most metallic elements and alloys approach $f \approx 0.5$ according to rather small variations of the density as expected for metals.

Topological properties and indices of the electron densities of Pd_2CoSe_2 and Na_2CoSe_2 are summarized in Table 5. The integrated charges Q_Ω differ strongly between Pd_2CoSe_2 and Na_2CoSe_2. Sodium is highly ionized ($Q_{Na} = +0.84$) and has almost the expected oxidation state +1, but palladium carries almost no charge ($Q_{Pd} = +0.06$). This is compensated by the much higher negative charge of selenium in Na_2CoSe_2 ($Q_{se} = -1.10$) compared to Pd_2CoSe_2 with only weakly polarized Se ($Q_{se} = 0.18$). Also the charge of the Co atoms is more than twice as high in Na_2CoSe_2 ($Q_{Co} = +0.53$) than in Pd_2CoSe_2 ($Q_{Co} = +0.25$). These properties are nicely reflected by the topological indices c and f. Na_2CoSe_2 with $c = 0.61$ and $f = 0.03$ appears to be a polar, almost salt-like compound. Nevertheless, a strictly ionic formulation $Na_2^+Co^{2+}Se_2^{2-}$ is only appropriate with respect to the Na^+ ions. Topologically, selenium is far from being Se^{2-} and also cobalt far from being Co^{2+}, therefore the $CoSe_{4/2}$ chains are better described as polyanions according to $Na_2^+[CoSe_2]^{2-}$. On the other hand, the very small charge-transfer index of Pd_2CoSe_2 ($c = 0.1$) shows any "forced" ionic formulation such as $Pd_2^+Co^{2+}Se_2^{2-}$ is far from reality. Interestingly, even though the charge transfer in Pd_2CoSe_2 is very low as expected for metallic materials, we do not find the typical high flatness of the density ($f \geqslant 0.5$). Rather than a uniform density distribution, $\rho(r)$ reaches high values of ~ 0.5 Å^{-3} at the BCP's of the Co–Se and Pd–Se bond paths and drops to 0.05 Å^{-3} in other regions of crystal space. However, this minimum is still five times larger than that in Na_2CoSe_2. Thus, the topological indices of the electron density classify the crystallographically isotypic compounds Na_2CoSe_2 and Pd_2CoSe_2 quantitatively as being very different materials from the viewpoint of chemical bonding and physical properties.

References

[1] H.F. Franzen, Prog. Solid State Chem. 12 (1978) 1–39.
[2] J.D. Corbett, J. Solid State Chem. 37 (1981) 335–351.
[3] H.F. Franzen, J. Solid State Chem. 64 (1986) 283–286.
[4] A. Simon, in: A.K. Cheetham, P. Day (Eds.), Solid State Chemistry Compounds, Oxford University Press, Oxford, 1992, pp. 112–165.
[5] T. Hughbanks, J. Alloys Compd. 229 (1995) 40–53.
[6] W. Tremel, H. Kleinke, V. Derstroff, C. Reisner, J. Alloys Compd. 219 (1995) 73–82.
[7] A. Simon, J. Alloys Compd. 229 (1995) 158–174.
[8] A.M. Ghorayeb, Key Eng. Mater. 155–156 (1999) 159–197.

[9] G. Gruener, A. Zettl, Phys. Rep. 119 (1985) 117–232.
[10] J. Rouxel, A. Meerschaut, L. Guemas, P. Gressier, Ann. Chim. Paris France 7 (1982) 445–457.
[11] M. Imada, A. Fujimori, Y. Tokura, Rev. Mod. Phys. 70 (1998) 1039–1263.
[12] S. Nagata, T. Atake, J. Therm. Anal. Calorim. 57 (1999) 807–821.
[13] C. Felser, R. Seshadri, Int. J. Inorg. Mat. 2 (2000) 677–685.
[14] A.P. Ramirez, R.J. Cava, J. Krajewski, Nature (London) 386 (1997) 156–158.
[15] A.L.N. Stevels, F. Jellinek, Monatsh. Chem. 102 (1971) 1679–1688.
[16] L.D. Gulay, I.D. Olekseyuk, J. Alloys Compd. 376 (2004) 131–138.
[17] P. Matkovic, K. Schubert, J. Less-Comm. Met. 52 (1977) 217–220.
[18] P. Matkovic, K. Schubert, J. Less-Comm. Met. 58 (1978) P39–P46.
[19] K. Cenzual, L.M. Gelato, M. Penzo, E. Parthe, Acta Crystallogr. B: Struct. Sci. B 47 (1991) 433–439.
[20] M. Janetzky, B. Harbrecht, Z. Anorg, Allg. Chem. 632 (2006) 837–844.
[21] S. Sato, T. Takabatake, M. Ishikawa, Acta Crystallogr. C: Cryst. Struct. Commun. C 45 (1989) 1–3.
[22] T. Takabatake, M. Ishikawa, J.L. Jorda, J. Less-Comm. Met. 134 (1987) 79–89.
[23] X-SHAPE, Crystal Optimization for Numerical Absorption Correction, Stoe & Cie GmbH, Darmstadt, 1999.
[24] X-RED32, X-RED Data Reduction, Stoe & Cie GmbH, Darmstadt, 2004.
[25] SHELXS, A Program for Crystal Structure Solution, 1997, Sheldrick, G.M., Universität Göttingen.
[26] SHELXL, A program for crystal structure refinement. Sheldrick, G.M., Universität Göttingen, 1997.
[27] P. Blaha, K. Schwarz, G.K.H. Madsen, D. Kvasnicka, J. Luitz, WIEN2k—An Augmented Plane Wave + Local Orbitals Program for Calculating Crystal Properties, TU Wien, 2001.
[28] K. Schwarz, P. Blaha, Comput. Mater. Sci. 28 (2003) 259–273.
[29] M. Kara, K. Kurki-Suonio, Acta Crystallogr. A: Found. Crystallogr. A 37 (1981) 201–210.
[30] E. Vielhaber, R. Hoppe, Z. Anorg. Allg. Chem. 360 (1968) 7–14.
[31] W. Bronger, C. Bomba, J. Less-Comm. Met. 158 (1990) 169–176.
[32] L. Pauling, Die Natur der chemischen Bindung, Verlag Chemie GmbH, Weinheim, 1976.
[33] J. Peters, B. Krebs, Acta Crystallographica, Section B: Structural Crystallography and Crystal Chemistry B 38 (1982) 1270–1272.
[34] Only the lattice constants of Na_2CoSe_2 are reported in [31]. The atomic coordinates of K_2CoSe_2 were used. Space group *Ibam*; a = 6.578 Å, b = 11.815 Å, c = 12.818 Å; Na: 0.3494 0.1488 0; Co: 0 0 0.25; Se 0.2029 0.8906 0. The FLAPW calculations converged without significant atomic forces, so no structure optimization was necessary.
[35] E.C. Stoner, Proc. Roy. Soc. (London) A 165 (1938) 372.
[36] E.C. Stoner, Proc. Roy. Soc. (London) A 169 (1939) 339–371.
[37] J.F. Janak, Phys. Rev. B 16 (1977) 255–262.
[38] R.F.W. Bader, Atoms in Molecules—A Quantum Theory, Oxford University Press, London, 1990.
[39] Y. Aray, J. Rodriguez, D. Vega, J. Phys. Chem. B 104 (2000) 4608–4612.
[40] P. Mori-Sanchez, A.M. Pendas, V. Luana, J. Am. Chem. Soc. 124 (2002) 14721–14723.